Energy-Based Fatigue Life Prediction of Composite Materials Using Thermoelastic Stress Analysis

Marques, Ricardo[1], Unel, Mustafa[2], Yildiz, Mehmet[2] and Suleman, Afzal[1]*

[1] *Department of Mechanical Engineering, Center for Aerospace Research, University of Victoria, Victoria, BC V8W 3P6, Canada.*

[2] *Integrated Manufacturing Technologies Research and Application Center, Sabanci University, Tuzla, 34956, Istanbul, Turkey.*
* Corresponding author (suleman@uvic.ca)

ABSTRACT

A remaining useful life (RUL) prediction routine was developed based on stored elastic strain energy density calculations using thermal data provided by the non-contacting and full-field capabilities of Thermoelastic Stress Analysis (TSA). Experiments were carried out on a quasi-isotropic E-glass fiber-reinforced polymer (GFRP) tensile specimen submitted to strain-controlled uniaxial fatigue loading conditions. A smoothing interpolation strategy using a two-dimensional quantic spline kernel function was applied to minimize over prediction of the fatigue lives at the crack front regions. An additional crack intensification factor (CIF) extended the effect of severe localized damage in the specimen's final RUL prediction. The initial state of the specimen was further used as the reference data for defining a damage parameter.

KEYWORDS: *Thermoelastic Stress Analysis, Composite materials, Remaining useful life, Strain energy density*

1 INTRODUCTION

During a flight mission, aircrafts are subjected to several fatigue loading scenarios, namely gust loads on the wings, inertial forces derived from maneuvers, or aerodynamic loads inherent to the fluid-structure interaction. In composite-based structures, although revealing higher fatigue strengths than metal-based, the dynamic behaviour of the aforementioned loads coupled with environmental effects and manufacturing-induced defects cause the onset and propagation of damage during the material's lifetime.

To minimize any negative impacts caused by the unexpected catastrophic failure of a structural component, Structural Health Monitoring (SHM) techniques can be employed to continuously acquire and process, in real-time, mechanical/thermal/electrical data captured through sensor systems, in order to ease the decision-taking process of repairing or replacing damaged parts. However, the strict regulatory demands within the framework of periodic monitoring of aircraft structures, and the engineering practicality of using traditional non-destructive inspection (NDI) techniques limit the widespread applicability of SHM techniques in the aerospace industry.

Thermoelastic Stress Analysis (TSA) is a non-contacting and non-destructive SHM technique that relies on the thermoelastic effect of solids deformed under reversible and quasi-adiabatic conditions to convert the full-field temperature differences captured by thermal cameras during a high-frequency dynamic test into first stress/strain invariant amplitudes. Main applications of TSA to composites range from qualitative and quantitative damage assessment (Fruehmann et al., (2010), Kakei et al., (2016)), to the identification of the measured thermoelastic signal's source (Emery et al (2008), Pitarresi and Galietti (2010), Pitarresi et al., (2005), Sambasivam and Dulieu-Barton, (2009)) and fatigue life prediction (Emery and Dulieu-Barton, (2010), Horn et al., (2001), Johnson et al., (2010)). The evolution of both Young's Modulus and first strain invariant change with the fatigue lifetime has been associated to the proximity to catastrophic failure, yet, in a qualitative perspective (Emery and Dulieu-Barton, (2010)), a stress concentration factor has been created based on the ratio between temperature differences measured in impacted and non-impacted regions, assuming that the location of damage is known beforehand (Horn et al., (2001)), and stochastic S-N curves have been obtained by combining TSA and the Markov Chain Method (Johnson et al., (2010)). However, fatigue life prediction using TSA-related articles lack of a more quantitative outcome without prior knowledge of damage location, thus opening opportunities for other approaches to tackle the problem.

In this work, a remaining useful life prediction routine based on the stepwise application of TSA during a composite material's fatigue lifetime is applied to the case of a quasi-isotropic E-glass fiber reinforced/epoxy matrix material, in order to simulate a real periodical maintenance scenario in a material typically implemented in non-critical aircraft structural elements. A theoretical background of the thermoelastic formulations and energy-based fatigue life prediction model are firstly presented, followed by a description of the material configuration, constituents, manufacturing method and relevant mechanical/thermal properties. The results discussion will also include a proposed quantitative measurement of the damage level imparted to the structure through a damage parameter independent of the *a priori* knowledge of its location.

2 THEORETICAL BACKGROUND

Composite manufacturing techniques lead to the accumulation of epoxy resin in the outer surface of the laminate, immediately after the first ply. It is stated in the literature that, at high frequencies, the temperatures being measured by the camera are derived from the epoxy layer, which acts as a strain-witness of the laminate (Salerno et al., (2009), Bakis and Reifsnider, (1991), Pitarresi et al.,(2005)). Therefore, the measured thermoelastic behaviour can be expressed in terms of the longitudinal strain change, $\Delta\varepsilon_{xc}$, according to the following equation valid for isotropic materials:

$$\frac{\Delta T}{T_0} = -\frac{\alpha_r}{\rho_r C_{pr}}\left[\frac{E_r}{1-\nu_r}\left(1-\nu_{xy}\right)\Delta\varepsilon_{xc}\right] \tag{1}$$

where ΔT is the temperature change between the peak points of a cyclic displacement/load change, T_0 is the absolute temperature at the mean point of the cycle, α_r is the coefficient of thermal expansion (CTE) of the resin, ρ_r is the density of the resin, C_{pr} is the specific heat at constant pressure of the resin, E_r is the resin's Young's modulus, ν_r is the Poisson's coefficient of the resin, and ν_{xy} is the composite's Poisson's ratio measured with respect to the global system of axes. To account for crack friction-based heating phenomena, a temperature correction methodology is implemented (Dulieu-Barton et al., (2006)). For the sake of practicality, $\overline{T}$ will hereinafter represent the temperature ratio, $\Delta T/T_0$.

The expended strain energy release rate (SERR), dU/dN, in composite materials subjected to constant strain amplitude conditions was found to be characterized by a distinct three-staged evolution until catastrophic failure is observed (Natarajan et al., (2005)). A power law relation between dU/dN and the applied-to-ultimate strain ratio ($\varepsilon_{max}/\varepsilon_{ult}$) has been developed by the same authors:

$$\frac{dU}{dN} = a\left(\frac{\varepsilon_{\max}}{\varepsilon_{ult}}\right)^{b} \qquad (2)$$

where a and b are coefficients which are function of geometrical, loading and material configurations. By integrating equation (2) between the ending and starting points of the fatigue life, the remaining useful life (RUL), N_t, at any moment of the fatigue life cycle can be obtained as:

$$N_t = \frac{u_0(r-1)}{0.75a(\varepsilon_{\max} / \varepsilon_{ult})^{b}} \qquad (3)$$

where r = u_f/u_0, u_0 represent the strain energy densities at the mean load/displacement level of a fatigue cycle calculated under the linear elastic stress-strain behavior assumption:

$$u_0 = \frac{1}{2}E_x \Delta\varepsilon_{xc}{}^{2} \qquad (4)$$

u_f is the strain energy density at the end of stage II of fatigue damage evolution – which is set to 90% of the total lifetime -, and the factor of 0.75 is a proposed correction with respect to the original RUL formulation (Natarajan et al., (2005)).

3 EXPERIMENTAL IMPLEMENTATION

3.1 Material Manufacturing and Characterisation

A quasi-isotropic (QI) configuration ($[0/45/-45/90]_s$) was manufactured using vacuum bagging of glass fiber prepregs on an aluminum mold. The prepreg was fabricated by Kordsa Company (with the code KOM10 EGF UD330) composed of stitched unidirectional E-glass fabric with a total areal weight of 330 g/m^2 from Metyx Composites and the epoxy resin with the code OM10. The process consisted in a first dwell period of 1h30 at 70 ^{0}C, followed by a second dwell period of 2h at 120 ^{0}C inside a temperature-controlled oven, with a final cool-down stage to avoid the generation of thermal residual stresses.

The relevant thermal-mechanical properties experimentally attained are presented in table 1. The value of C_{pr} was obtained for a temperature equal to the harmonic average of all pixel's T_0 at the undamaged state. The r value in equation 3 was selected depending upon the chosen $\varepsilon_{max}/\varepsilon_{ult}$ for fatigue testing using a power law fitting curve's equation.

Table 1 - GFRP's and epoxy's material properties.

Property	**Unit**	**Value**
ε_{ult}	%	2.59
ρ_r	Kg/m^3	1142
C_{pr}	J/(Kg.^{0}C)	1290
E_r	GPa	3.08
ν_r	--------	0.35
a | b	J/(m^3.cycle) | -----	4619.5 | 7.4298
α_r	^{0}C^{-1}	6.60 x 10^{-5}

3.2 Procedure

The adopted strategy for implementation is schematically shown figure 1.

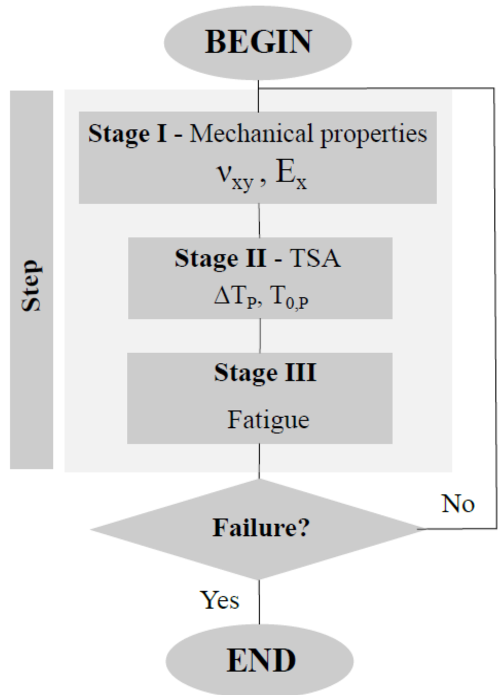

Figure 1 – Schematic of the experimental procedure for RUL prediction.

An initial determination of E_x and ν_{xy} through a quasi-static tensile test was conducted in accordance with the ASTM D3039 recommendations. In the next stage, TSA was performed under strain-controlled conditions using a dynamic extensometer. Cyclic strain limits were kept between 2-15% of ε_{ult}, a frequency of 12 Hz assured adiabatic conditions, and a total of 1200 cycles per test contributed for improving the signal-to-noise ratio. Thermal images were captured using a FLIR X6580sc model, with a 25 mm lens installed, and positioned at a stand-off distance of 570 mm with respect to the specimen. The Edevis DisplayImg 6 software enabled data acquisition and visualization after completion. In the final fatigue stage, damage was allowed to evolve at a maximum applied strain level imposed by the TSA's maximum strain in order to remain valid the process behind the u_0 calculation. Therefore, the dynamic strain change was kept at $\varepsilon_{max}/\varepsilon_{ult}$ equal to 0.28 for 20000 cycles, where a 5 Hz frequency assured no temperature-induced effects on the fatigue life of the specimen. The r value was determined to be 1.71. The aforementioned three stages are repeated in a stepwise manner until a failure condition is met.

4 RESULTS AND DISCUSSION

4.1 Remaining Useful Life Prediction

Since E_x and ν_{xy} are representative values of the whole specimen, a unique global value for the RUL at each step, s, is attained based on the harmonic averaging of the pixel-wise temperature ratios, $<\bar{T}_g^{(s)}>$:

$$\frac{1}{<\bar{T}_g^{(s)}>} = \frac{1}{p}.\sum_{i=1}^{p}\frac{1}{\bar{T}_i^{(s)}} \tag{5}$$

where p stands for the total number of pixels considered for averaging.

In order to better approximate the RUL predictions to the physical reality of fatigue damage phenomena, two post-processing methodologies were applied to the original collected data. One can separate a damage or crack into two regions according to their thermoelastic response, namely the crack surface and the immediate vicinity of the crack front. It was observed that the material discontinuity between crack surfaces leads to a reduction in the elongation level of the crack surfaces in response to a cyclic external load or deformation, yielding lower $\bar{T}$ and N_t. On the other hand, at the crack fronts, the enhanced tendency for the material to separate leads to higher deformation levels represented by locally higher $\bar{T}$ values which consequently lead to an unrealistic increase in the fatigue lives.

To circumvent and minimize overprediction of fatigue lives at the crack fronts, the thermoelastic response at the crack surfaces was extended into the crack fronts. To this end, we utilized a smoothing or interpolation methodology using a two-dimensional quintic spline kernel function (Shadloo et al., (2013)) considering the smoothing length as h = 2Δx, and the maximum radius of influence centered in the pixel of interest, R = 3h, where Δx is the physical distance between pixels defined as $1/n_p$, being n_p the total number of pixels along the specimen's width direction. Assuming that step 0 is the material's undamaged state, this methodology has only been applied from step 1 onwards.

Moreover, to extend the influence of the very-localized damaged regions into the intact ones, and weight the impact of these regions in the structural failure state, a crack intensification factor (CIF), Γ, was added to equation 3, after smoothing is performed:

$$N_t = \frac{u_0(r-1)}{0.75a(\varepsilon_{\max}/\varepsilon_{ult})^b}.\Gamma_s^{bx_s} \tag{6}$$

where $x_s = N_s/N_u$ is the fraction of the fatigue cycles at each TSA step, N_s is the total number of cycles up to step s, and N_u is the equivalent to N_t defined at the undamaged state using the weighted harmonic average of temperature ratios before smoothing.

A total of 17 steps - equivalent to 327,630 fatigue cycles – were performed. The comparison of RUL life predictions obtained using the original thermoelastic data (denoted as BS), temperature data modified by the smoothing process (denoted as AS), and by incorporating the CIF in the initial formulation with respect to a reference line which reflects a theoretical linear fatigue life decay are plotted in figure 2. In the early steps, none of the approaches yield acceptable predictions, owing to the incapability of the models to counteract the sudden longitudinal stiffness decay that is observed at this stage. As we progress towards the intermediate stage of the fatigue lifetime, excellent predictions were attained using the BS and AS approaches, namely between steps 5 and 9. However, as more localized damages form and grow, results tend to deviate and over predict with respect to the reference curve, thus the requirement for correction using the CIF. To account for the benefits of both smoothing and CIF implementations as corrective schemes, a harmonic average of each model's predictions at each step was performed, thus yielding the final prediction curve, also represented in figure 2. Excellent agreement can be found between the final and reference curves from step 10 onwards, while providing conservative results before reaching that step.

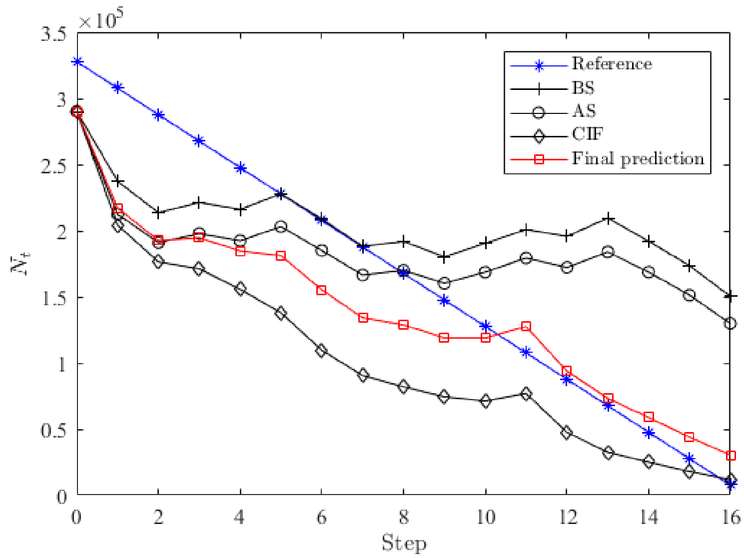

Figure 2 - Comparison between the reference and calculated N_t.

4.2 Damage Parameter

For step s, a non-dimensional parameter, $D_p^{(s)}$, was defined by the ratio between the local number of cycles until failure, $N_{t,p}^{(s)}$, and the harmonic averaged RUL determined at the undamaged reference state, $<N_t^{(0)}>$:

$$D_p^{(s)} = 1 - \frac{N_{t,p}^{(s)}}{<N_t^{(0)}>} = 1 - \frac{C_{pr,p}^{(s)} \Delta T_p^{(s)}}{C_{pr}(<T_0^{(0)}>) <\Delta T^{(0)}>} \tag{7}$$

where $<\Delta T^{(0)}>$ is the harmonic averaged temperature change at the undamaged state, $C_{pr,p}^{(s)}$ is the pixel-wise value of specific heat at constant pressure at step s, $\Delta T_p^{(s)}$ is the pixel-wise temperature change at step s, and $C_{pr,}(<T_0^{(0)}>)$ is the specific heat at constant pressure calculated from the harmonic averaged mean absolute temperature at the undamaged state. The purpose of this parameter was to provide a feasible comparison in a real maintenance scenario where the actual number of cycles until failure is unknown. Full-field plots for steps 4, 8, 12 and 16 together with the specimen's final configuration are shown in Fig. 7. Damage visually perceived is demarcated inside a red box and detectable by an increased D value at the same location namely during the last performed step. Moreover, subsurface damage is also detected thus highlighting the TSA's capability to assess damage through-the-thickness.

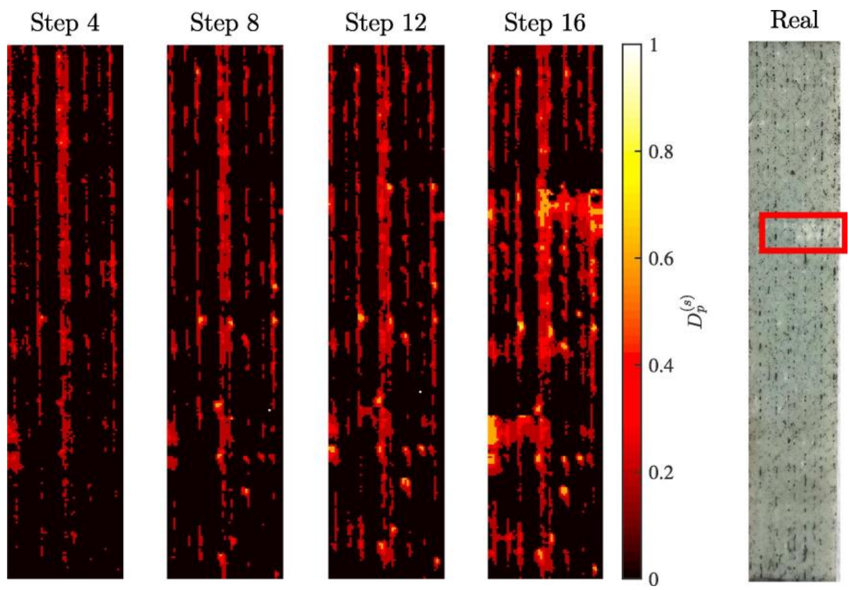

Figure 3 – Damage parameter evolution.

5 CONCLUSION

A novel TSA-based RUL estimation using the strain energy density was developed and successfully implemented on an initially undamaged quasi-isotropic E-glass fiber-reinforced composite laminate. The initial rapid stiffness degradation coupled with the formation and growth of cracks in very small localized regions compared with the overall specimen dimension led to a deviation of the calculated N_t results from the reference linear curve within the initial and final steps. For more realistic predictions, the effect of damage in crack regions was extended to the remaining structure through a multiplicative crack intensification factor included in the firstly-derived RUL equation. It is shown that this method improved the attained results during the end of the intermediate and last fatigue life stages. Moreover, a damage parameter based on the evolution of minimum value of pixel-wise strain energy density has been proposed. Unaware of the total number of fatigue cycles, the TSA full-field capability enabled the determination of the severity and quantification of the crack responsible for final failure using a damage parameter.

6 ACKNOWLEDGEMENTS

The financial and infrastructural support provided by Sabanci University – Integrated Manufacturing Technologies Research and Application Center and Sabanci University – Kordsa Composite Technologies Center of Excellence is greatly acknowledged. Afzal Suleman acknowledges the NSERC Canada Research Chair funding.

REFERENCES

Bakis, C. E., & Reifsnider, K. L. (1991). The adiabatic thermoelastic effect in laminated fiber composites. Journal of composite materials, 25(7), 809-830.

Dulieu-Barton, J. M., Emery, T. R., Quinn, S., & Cunningham, P. R. (2006). A temperature correction methodology for quantitative thermoelastic stress analysis and damage assessment. Measurement Science and Technology, 17(6), 1627.

Emery, T. R., & Dulieu-Barton, J. M. (2010). Thermoelastic stress analysis of damage mechanisms in composite materials. Composites Part A: Applied Science and Manufacturing, 41(12), 1729-1742.
Emery, T. R., Dulieu-Barton, J. M., Earl, J. S., & Cunningham, P. R. (2008). A generalised approach to the calibration of orthotropic materials for thermoelastic stress analysis. Composites Science and Technology, 68(3-4), 743-752.
Fruehmann, R. K., Dulieu-Barton, J. M., & Quinn, S. (2010). Assessment of fatigue damage evolution in woven composite materials using infra-red techniques. Composites Science and Technology, 70(6), 937-946.
Horn, G. P., Mackin, T. J., & Kurath, P. (2001). Estimating the residual fatigue lifetimes of impact-damaged composites using thermoelastic stress analysis. Polymer composites, 22(3), 420-431.
Johnson, S., Wei, B., & Haj-ali, R. (2010). A stochastic fatigue damage model for composite single lap shear joints based on Markov chains and thermoelastic stress analysis. Fatigue & Fracture of Engineering Materials & Structures, 33(12), 897-910.
Kakei, A., Epaarachchi, J. A., Islam, M., Leng, J., & Rajic, N. (2016). Detection and characterisation of delamination damage propagation in Woven Glass Fibre Reinforced Polymer Composite using thermoelastic response mapping. Composite Structures, 153, 442-450.
Natarajan, V., Gangarao, H. V., & Shekar, V. (2005). Fatigue response of fabric-reinforced polymeric composites. Journal of composite materials, 39(17), 1541-1559.
Pitarresi, G., Found, M. S., & Patterson, E. A. (2005). An investigation of the influence of macroscopic heterogeneity on the thermoelastic response of fibre reinforced plastics. Composites Science and Technology, 65(2), 269-280.
Pitarresi, G., & Galietti, U. (2010). A quantitative analysis of the thermoelastic effect in CFRP composite materials. Strain, 46(5), 446-459.
Salerno, A., Costa, A., & Fantoni, G. (2009). Calibration of the thermoelastic constants for quantitative thermoelastic stress analysis on composites. Review of Scientific Instruments, 80(3), 034904.
Sambasivam, S., Quinn, S., & Dulieu-Barton, J. M. (2009). Identification of the source of the thermoelastic response from orthotropic laminated composites.
Shadloo, M. S., Rahmat, A., & Yildiz, M. J. C. M. (2013). A smoothed particle hydrodynamics study on the electrohydrodynamic deformation of a droplet suspended in a neutrally buoyant Newtonian fluid. Computational Mechanics, 52(3), 693-707.